

RNNPool: Efficient Non-linear Pooling for RAM Constrained Inference

Oindrila Saha¹ Aditya Kusupati² Harsha Vardhan Simhadri¹ Manik Varma¹ Prateek Jain¹

Abstract

Pooling operators are key components in most Convolutional Neural Networks (CNNs) as they serve to downsample images, aggregate feature information, and increase receptive field. However, standard pooling operators reduce the feature size gradually to avoid significant loss in information via gross aggregation. Consequently, CNN architectures tend to be deep, computationally expensive and challenging to deploy on RAM constrained devices. We introduce RNNPool, a novel pooling operator based on Recurrent Neural Networks (RNNs), that efficiently aggregate features over large patches of an image and rapidly downsamples its size. Our empirical evaluation indicates that an RNNPool layer(s) can effectively replace multiple blocks in a variety of architectures such as MobileNets (Sandler et al., 2018), DenseNet (Huang et al., 2017) and can be used for several vision tasks like image classification and face detection. That is, RNNPool can significantly decrease computational complexity and peak RAM usage for inference while retaining comparable accuracy. Further, we use RNNPool to construct a novel real-time face detection method that achieves state-of-the-art MAP within computational budget afforded by a tiny Cortex M4 microcontroller with ~ 256 KB RAM.

1. Introduction

Pooling operators generate aggregate representations of features corresponding to a spatial region and are commonly used in CNNs to down-sample activation maps. For example, DenseNet121 (Huang et al., 2017) uses 5 pooling layers and ResNet18 (He et al., 2016) uses 2 pooling layers. While MobileNetV2 (Sandler et al., 2018) and EfficientNet (Tan & Le, 2019) do not have explicit pooling layers, they use strided convolutions to down-sample the image, which can also be viewed as a weighted average pooling.

¹Microsoft Research, India ²University of Washington, USA.
Correspondence to: Prateek Jain <prajain@microsoft.com>.

Typical pooling operators use computationally efficient but gross aggregation methods like (weighted) average or maximum of the inputs, which restricts their application to a small receptive field (typically < 4). As a result, to downsample layers and to increase the receptive fields of downstream neurons, multiple stacks of convolutions (or requirement operations) and pooling operators are needed. For example, DenseNet121 uses 41 layers to reduce size of the image from 112×112 to 14×14 . Similarly, MobileNetV2 requires 19 layers for the same task.

This results in deep and large models that are computationally expensive for inference. Recently, several techniques have been proposed to reduce the inference cost while retaining the depth of the architecture. These include quantization or sparsification of the parameters (Wang et al., 2019; Gale et al., 2019), cheaper CNN blocks (Sandler et al., 2018; Iandola et al., 2016), or architecture search (Tan & Le, 2019).

However, due to the large number of layers and dense residual connections in these new architectures, their working-memory requirement for inference is large. This is a major issue for real-time inference on battery-powered and other resource-constrained devices which tend to have small RAM to save power (e.g. ARM Cortex M4-based devices typically have about 256 KB RAM). Consider, for example, the face detection task with 640×640 sized inputs. MobileNetV2 would require 18 layers to bring down the size of the image down to say 80×80 with about 32 channels. If the RAM is constrained to $80 \times 80 \times 32$ (i.e. ≈ 200 KB), then we cannot store the output of the intermediate layers. As a result, individual entries of the 28×28 output would need to be evaluated one at a time, using expensive re-computation of large parts of the 18 intermediate layers.

In this paper, we propose RNNPool, a novel pooling operator that uses Recurrent Neural Network (RNN) to perform a more refined aggregation of large patches without a significant reduction in accuracy. While RNNPool can be applied to any tensor structured problem, for ease of exposition we focus only on 2D images. For images, RNNPool applies RNNs both along rows and columns and then combines them to compute a fine aggregation of the given pool/patch of features. RNNPool has three parameters – patch-size or pooling receptive field size, stride, and output dimension – that control its expressiveness and down-sampling ability.

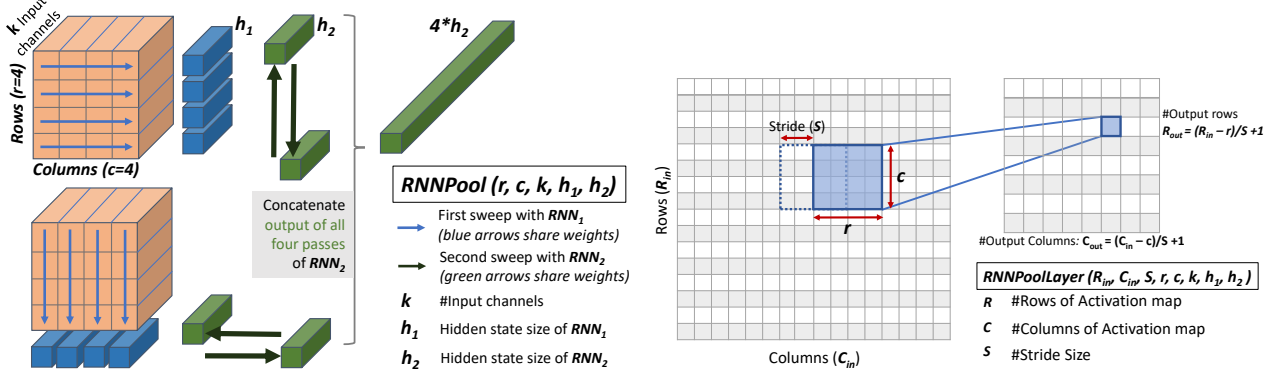


Figure 1. (left) An RNNPool operator. (right) An RNNPoolLayer composed with strided RNNPool operators with shared weights.

Using RNNPool, we can rapidly down-sample images and activation maps, eliminating the need for many residual blocks in the CNN architectures. This reduces the working memory requirement significantly. RNNPool is most effective when used to replace multiple blocks in the initial stages of the model that reduces the size of large activation maps (and thus need most memory and compute). There, it can down-sample by a factor of 4 or 8 with just one layer. For example, RNNPool applied to a 3 channel 640×640 image with patch-size 16, stride 8, and 32 output channels results in an activation map of size $80 \times 80 \times 32$. This map can be stored in ~ 200 KB memory. So in addition to reducing compute, this replacement brings down the peak memory requirement to similar value for typical architectures.

Our experiments demonstrate that RNNPool can indeed be used as an effective replacement for deep expensive functional blocks in a variety of architectures such as MobileNet, DenseNet, EfficientNet, and can be used in different tasks like image classification and face detection. For example, in a 10-class image classification task, RNNPool +MobileNetV2 helps reduce the peak RAM usage of MobileNetV2 by up to $10\times$ and the FLOPs by about 25%, while maintaining the *same* accuracy. Furthermore, due to its general formulation, it can replace individual pooling layers at all stages of CNN. For example, it can replace the final average pooling layer in architectures like MobileNetV2 and improve accuracy by $\sim 1\%$.

Finally, we develop a new class of architectures for face detection using RNNPool with MobileNetV2 that can train: (a) a model which needs only 225KB working memory – small enough to be deployed on a Cortex M4 based device – but achieves 0.80 and 0.78 MAP on the easy and medium categories of the WIDER FACE dataset, and (b) a model that can beat start-of-the-art accuracy with $5\times$ fewer FLOPs.

In summary, we make the following contributions:

- A novel pooling operator that can rapidly downsample images and can be used to reduce depth of a variety of

standard architectures, e.g., MobileNetV2, DenseNet121.

- Demonstrate that RNNPool can reduce memory and compute requirement for tasks like image classification and Visual Wake Words while retaining comparable accuracy.
- Develop new architectures for face detection that push the boundary of Mean Average Precision (MAP) vs working memory and compute requirement.

2. Related Work

Pooling: Max-pooling, Average-pooling and strided convolution layers (LeCun et al., 2015) are standard techniques for feature aggregation and for reducing spatial resolution in DNNs. Existing literature on rethinking pooling (Zhao et al., 2018; He et al., 2015; Gong et al., 2014) focuses mainly on increasing accuracy. But it does not take compute/memory efficiency into consideration which is one of the primary focus of this paper and the RNNPool operator.

Efficient CNN architectures: Most existing research on design of efficient CNN models aims at reducing inference cost (FLOPs) and model size. The methods include designing new model architectures such as DenseNet (Huang et al., 2017), MobileNets (Howard et al., 2017; Sandler et al., 2018) or searching for them (e.g. ProxylessNAS (Cai et al., 2018), EfficientNets (Tan & Le, 2019)). The aforementioned models do not optimize the peak working memory (RAM) of the model, which can be a critical constraint on tiny devices like microcontrollers. Previous work on memory (RAM) optimized inference manipulates existing convolution operator by reordering computations (Cho & Brand, 2017; Lai et al., 2018) or performing them in-place (Gural & Murmann, 2019) to save storage. However, most of these methods provide relatively small memory savings and typically apply to small images like in CIFAR-10 (Krizhevsky et al., 2009). In contrast, RNNPool reduces memory requirement significantly while maintaining accuracy on various real-world vision tasks and benchmarks.

Visual Wake Words: Visual cues (visual wake word) to “wake-up” AI-powered home assistant devices require real-time inference on relatively small devices. Chowdhery et al. (2019) proposed a Visual Wake Words dataset and a resource-constrained setting to evaluate various methods. They benchmarked modified versions of MobileNetV1, MobileNetV2 and MnasNet (Tan et al., 2019) to fit within the problem budget. In Section 5.2, we show that an RNNPool based MobileNetV2 architecture can enable solutions with comparable accuracy to the prior art but in about $8\times$ less RAM and 40% lower compute cost (FLOPs).

Face-detection on tiny devices: Many recent works including EXTD (Yoo et al., 2019), LFFD (He et al., 2019), FaceBoxes (Zhang et al., 2017a) and EagleEye (Zhao et al., 2019) address the problem of real-time face detection on resource-constrained devices. EXTD and LFFD are the most accurate but have high compute and memory requirements. On the other hand, EagleEye and FaceBoxes have lower inference complexity but also suffer from lower MAP scores. We propose an RNNPool based architecture that can potentially be deployed on Cortex M4 class devices while still ensuring 5-10% higher accuracy than EagleEye.

RNNs for vision tasks: Recurrent Neural Networks (RNNs) have been the go-to solutions for sequential tasks but haven’t been extensively explored in the context of computer vision. An early work, ReNet (Visin et al., 2015) uses RNN based layer as a replacement for a convolution layer but does not aim at improving efficiency. ReNet results in larger model size and FLOPs if the input and output dimensions are set the same as that of an RNNPool layer. PolygonRNN (Acuna et al., 2018), CNN-RNN (Wang et al., 2016) and Conv-LSTM (Xingjian et al., 2015) also use RNNs in their model architecture but only to model certain sequences in the respective tasks rather than tackling pooling and efficiency of the architecture.

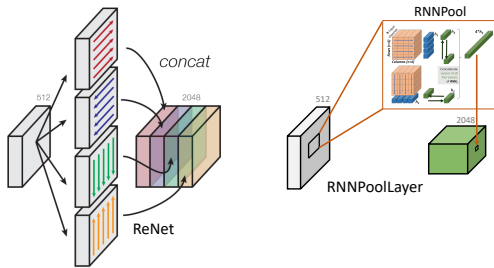


Figure 2. Comparison of a ReNet based spatial RNN layer (left) (figure from (Bell et al., 2016)) with our RNNPoolLayer (right)

RNN as a spatial operator: Since ReNet (Visin et al., 2015), there have been many methods which have been built upon it to solve various vision tasks. The fundamental difference, mathematically, between these approaches and ours is how the RNN is used to extract spatial information.

In ReNet based methods, the RNN is used to find a pixel-wise mapping from a voxel of the input activation map to that of the output map. However, in our method, we are using RNNs to spatially summarize a big patch of the input activation map to a 1×1 voxel of the output activation map. Further, Figure 2 shows the difference between how the outputs of the RNN are being used. Note that in ReNet the hidden states of every timestep of RNN contribute to one voxel of the output, whereas in our case only the last hidden states of the traversals are taken for both row/column-wise summarizations and bidirectional summarizations. A problem with using every hidden state to determine the output as in ReNet is that the earlier hidden states do not contain significant information as compared to the last one i.e. the information keeps accumulating till the last timestep. This will create a bias towards the boundaries for a ReNet like layer since there are bidirectional passes all over the image. However, such a problem can’t be seen in our approach as we always take the final hidden state of the whole pass. ReNet based approaches are either inserting their RNN based layers in existing networks or are replacing a single convolution layer with the same (thus resulting in increasing computations). Our usage of RNN for spatial information extraction is so powerful that we can replace a huge number of convolution layers and still preserve accuracy. Most importantly, we significantly decrease RAM usage since we are summarizing and reducing the spatial resolution as compared to performing a pixel to pixel mapping. Also, we see a decrease in FLOPs while ReNet based methods will increase the FLOPs of the baseline model.

Inside-Outside Net (Bell et al., 2016) also uses a ReNet based RNN layer for extracting context features in object detection while PiCANet (Liu et al., 2018) uses it as a global attention function for salient object detection. L-RNN (Xie et al., 2016) inserts multiple ReNet based layers but in a cascading fashion i.e. first horizontal passes, then vertical passes on the resulting map. These methods have been evaluated on tasks like CIFAR-10 classification and semantic segmentation.

Note that in all the above applications, the RNNs are applied over the whole input map, whereas we are doing computations patch by patch, more like a pooling operator. ReNet also proposes using patches to decrease resolution, but the existing methods flatten it to one big 1×1 voxel and using it as a single timestep input to the RNN, which results in loss of spatial dependencies.

3. What is RNNPool?

Consider the output of an intermediate layer in a CNN of size $R \times C \times f$, where f is the number of features or channels. A layer of typical 2×2 pooling operators (e.g. max or average) with stride 2 would halve the number of rows (R)

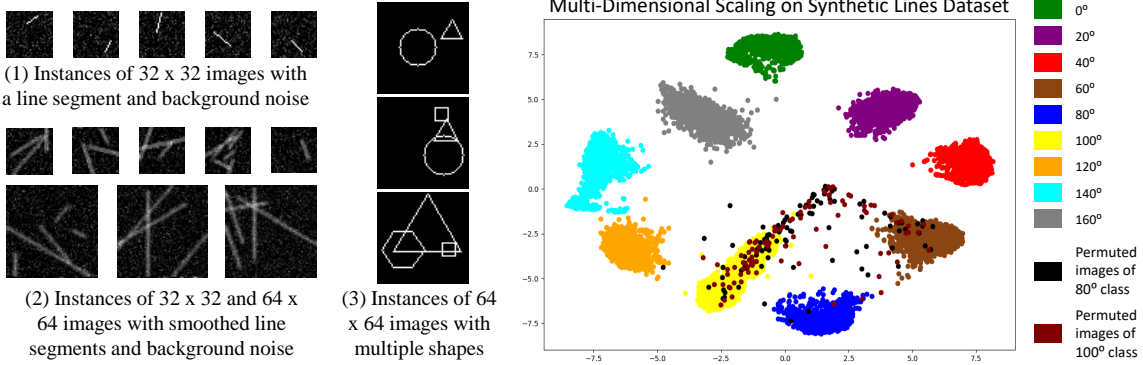


Figure 3. (left) Examples from three multi-class and multi-label synthetic datasets used for probing RNNPool. (right) A 2-dimensional Multi-Dimensional Scaling visualization of the 128 dimensional output of RNNPool operator for the multi-class dataset (1). Some test images (plotted using black and brown dots) were modified by randomly permuting rows and columns.

and columns (C). Therefore, reducing the dimensions by a factor of 4 would require two blocks: a stack of convolutions to capture key features in the image and a pooling layer. Our goal is to reduce the activation of size $R \times C \times f$ to, say, $R/4 \times C/4 \times f'$ in a single layer while retaining the information necessary for the downstream task. We do so using an RNNPoolLayer illustrated in Figure 1 that utilizes strided RNNPool operators.

3.1. The RNNPool Operator and the RNNPoolLayer

An RNNPool operator of size (r, c, k, h_1, h_2) takes as input an activation patch of size $r \times c \times k$ corresponding to k input channels, and uses a pair of RNNs – RNN_1 of hidden dimension h_1 and RNN_2 with hidden dimension h_2 – to sweep the patch horizontally and vertically to produce a summary of size $1 \times 1 \times 4h_2$.

Algorithm 1 explains the details of RNNPool operator. The RNNPool applies two parallel pipelines to the patch and concatenates their outputs. The first is where RNN_1 traverses along rows and summarizes the patch horizontally (Line 12) and then RNN_2 passes through the outputs of RNN_1 (Lines 13–14) bi-directionally. In the second pipeline RNN_1 first traverses along columns to summarize the patch vertically (Line 15) and then RNN_2 (Lines 16–17) summarizes bi-directionally.

While it is possible to use GRU (Cho et al., 2014) or LSTM (Hochreiter & Schmidhuber, 1997) for the two instances of RNN in RNNPool, we use FastGRNN (Kusupati et al., 2018) for its compact size and fewer FLOPs.

An RNNPoolLayer consists of a single RNNPool operator strided over an input activation map. Note that there are only two RNNs (RNN_1 & RNN_2) in an RNNPool operator, thus weights are shared for both the row-wise and column-wise passes (RNN_1) and all bi-directional passes (RNN_2).

Algorithm 1 RNNPool Operation

Input: $\mathbf{X} : [\mathbf{X}_{1,1} \dots \mathbf{X}_{r,c}] ; \mathbf{x}_{i,j} \in \mathcal{R}^k$
Output: $\text{RNNPool}(r, c)$

```

1: function FastGRNN( $\mathcal{P}, \mathbf{x}$ )
2:    $[\mathbf{W}, \mathbf{U}, \mathbf{b}_z, \mathbf{b}_h] \leftarrow \mathcal{P}$ ,  $\mathbf{h}_0 \leftarrow \text{randn}$ 
3:   for  $k \leftarrow 1$  to  $\text{length}(\mathbf{x})$  do
4:      $\mathbf{z} \leftarrow \sigma(\mathbf{W}\mathbf{x}_k + \mathbf{U}\mathbf{h}_{k-1} + \mathbf{b}_z)$ 
5:      $\tilde{\mathbf{h}}_k \leftarrow \tanh(\mathbf{W}\mathbf{x}_k + \mathbf{U}\mathbf{h}_{k-1} + \mathbf{b}_h)$ 
6:      $\mathbf{h}_k \leftarrow \mathbf{z} \odot \mathbf{h}_{k-1} + (1 - \mathbf{z}) \odot \tilde{\mathbf{h}}_k$ 
7:   end for
8:   return  $\mathbf{h}_T$ 
9: end function

10:  $\text{RNN}_i(\cdot) \leftarrow \text{FastGRNN}(\mathcal{P}_i, \cdot)$ , for  $i \in \{1, 2\}$ 
11: function RNNPool( $\mathbf{X}$ )
12:    $\mathbf{p}_i^r \leftarrow \text{RNN}_1(\mathbf{X}_{i,1 \leq j \leq c})$ , for all  $1 \leq i \leq r$ 
13:    $\mathbf{q}^{r_1} \leftarrow \text{RNN}_2(\mathbf{p}_1^h)$ 
14:    $\tilde{\mathbf{p}}^r \leftarrow \text{reverse}(\mathbf{p}^r)$ ,  $\mathbf{q}^{r_2} \leftarrow \text{RNN}_2(\tilde{\mathbf{p}}_1^h)$ 
15:    $\mathbf{p}_j^c \leftarrow \text{RNN}_1(\mathbf{X}_{1 \leq i \leq r,j})$ , for all  $1 \leq j \leq c$ 
16:    $\mathbf{q}^{c_1} \leftarrow \text{RNN}_2(\mathbf{p}_1^c)$ 
17:    $\tilde{\mathbf{p}}^c \leftarrow \text{reverse}(\mathbf{p}^c)$ ,  $\mathbf{q}^{c_2} \leftarrow \text{RNN}_2(\tilde{\mathbf{p}}_1^c)$ 
18:   return  $[\mathbf{q}^{r_1}, \mathbf{q}^{r_2}, \mathbf{q}^{c_1}, \mathbf{q}^{c_2}]$ 
19: end function

```

across every instance of RNNPool in an RNNPoolLayer. Further, RNNPoolLayer also takes two more parameters into account: patch size and the stride length.

3.2. Capturing Edges, Orientations and Shapes

To probe RNNPool’s efficacy at capturing edges, orientation and shapes, we first fit an RNNPool operator to the synthetic datasets of small 8-bit monochrome images with background noise as shown in Figure 3. We observe that a single RNNPool module fits to 100% accuracy on these datasets. The details of the experiments are in the Appendix B.

Further, we use multi-dimensional scaling to visualize the $4 \cdot h_2 = 128$ dimensional output of RNNPool operator on the multi-class dataset (1) in Figure 3 (left). Dataset (1) consists of various lines in the image at a discrete set of angles, and the classification task is to detect the angle of the line. Some images from the test set of classes 80° and 100° are multiplied with a permutation matrix to randomly permute rows and columns. These resulting images are added to the original test dataset and the output of the RNNPool is plotted in Figure 3 (right). The outputs for each class form well-separated tight clusters indicating RNNPool indeed learns various orientations, while the outputs for the permuted images are scattered across the plot indicating that it is not exploiting certain gross aggregations in the data.

We also conclude that the horizontal and the vertical passes of the RNN allows a single RNNPool operator to capture the orientation of edges and simple shapes over patches of size up to 64×64 . Further, adding a single convolutional layer before the RNNPool layer makes the model much more parameter efficient (see Appendix B). In effect, the convolution layer detects gradients in a local 3×3 patch, while the RNNPool detects whether gradients across 3×3 patches aggregate into a target shape.

3.3. Comparing Performance with Pooling Operators

We now contrast the down-sampling power of RNNPool against standard pooling operators. That is, we investigate if the pooling operators maintain accuracy for a downstream task even when the pooling receptive field is large. To this end, we consider the image classification task with CIFAR-10 dataset but the pooling operator is required to down-sample the input 32×32 image to a 1×1 voxel in *one go* i.e. both patch size and stride are 32. This is followed by a fully connected (FC) layer. The number of output channels after pooling was ensured to be the same. For Max and Average pooling models, a 1×1 convolution is used to ensure the same output dimension. For this task, RNNPool achieves an accuracy of **70.63%**, while convolution layer, max pooling and average pooling’s accuracy are 53.13%, 20.04% and 26.53%, respectively. This demonstrates the modeling power of the RNNPool operator over other pooling methods. Table 1 (Rows 2-5) reinforces the same but on bigger image classification datasets.

4. How to use the RNNPoolLayer?

RNNPool can be used to modify several state-of-the-art architectures to reduce their working memory as well as computational requirements. Typically, such modifications involve replacing one or more stacks of convolutional and pooling layers of the “base” (original) architecture with an RNNPoolLayer and retraining from scratch. We demonstrate modification strategies here and demonstrate their ef-

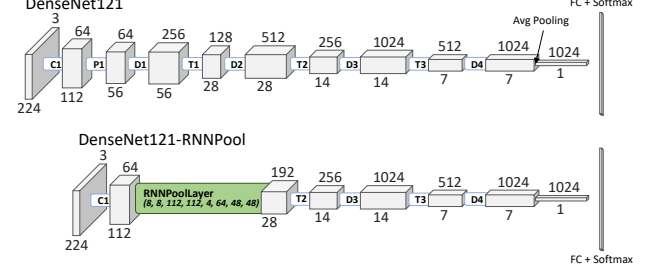


Figure 4. **DenseNet121-RNNPool**: obtained by replacing P1, D1, T1 and D2 blocks in DenseNet121 with an RNNPoolLayer.

fectiveness through extensive experimentation in Section 5.

4.1. Replacement for a Sequence of Blocks

Consider the DenseNet121 (Huang et al., 2017) architecture in Figure 4. It consists of one convolutional layer, followed by repetitions of “Dense” (D), transition (T) and pooling (P) blocks which gradually reduce the size of the image while increasing the number of channels. Of all these layers, the first block following the initial convolutional layer – D1 – requires the maximum working memory and FLOPs – 3.06 MB and 1.04 GFLOPs to be precise, if we disallow any re-computation of intermediate value – as it deals with large activation maps that are yet to be downsampled. Furthermore, the presence of residual connections between all 6 layers within each dense block exacerbates the memory management problem¹. This property is also true of other architectures with residual connections such as MobileNetV2, EfficientNet and ResNet.

We can use an RNNPoolLayer to rapidly downsample the image size and bypass intermediate large spatial resolution activations. In DenseNet121, we can replace 4 blocks - P1, D1, T1, D2 - spanning 39 layers with a single RNNPoolLayer to reduce the activation map from size 112×112 to 28×28 (see Figure 4). The replacement RNNPoolLayer can be executed patch-by-patch without re-computation, thus reducing the need to store the entire activation map across the image. These two factors contribute greatly to the reduction in working memory size as well as the number of computations. DenseNet121-RNNPool achieves an accuracy of 94.8% on ImageNet-10 which is comparable to 95.4% of the original DenseNet121 model.

A similar replacement of functional blocks with RNNPoolLayer can be performed for MobileNetV2 as specified in Table 2. As a result, the working memory

¹If no re-computation is allowed, residual connections force us to store each intermediate layer in working memory. On the contrary, if there were no residual connections in the dense block, the working memory would be proportional to the size of the convolution and number of layers and not the image size

Table 1. ImageNet-10 classification and Visual Wake Words tasks with few base layers replaced by different pooling strategies. Row 5 refers to RNNPool Block utilized as shown in Table 2 for MobileNetV2 and Figure 4 for DenseNet121. Average Pooling, Max Pooling and Strided Convolutions are used to replace the blocks in the base network at the same position as RNNPool was used in Row 5. Last layer RNNPool (Row 6) replaces the last Average Pooling layer in the models. The last row of the table refers to the replacement of blocks as in Row 5 along with the last Average Pooling layer in the base network with RNNPoolLayer.

Method	ImageNet-10						Visual Wake Words		
	MobileNetV2			DenseNet121			MobileNetV2-0.35×		
	Accuracy (%)	FLOPs	Parameters	Accuracy (%)	FLOPs	Parameters	Accuracy (%)	FLOPs	Parameters
Base Network	94.20	0.300G	2.2M	95.40	2.83G	6.96M	90.20	53.2M	296K
Average Pooling	90.80	0.200G	2.0M	92.80	0.71G	5.59M	86.85	31.9M	255K
Max Pooling	92.80	0.200G	2.0M	93.40	0.71G	5.59M	86.92	31.9M	255K
Strided Convolution	93.00	0.258G	2.1M	93.80	1.33G	6.38M	88.08	39.2M	264K
RNNPool Block	94.40	0.226G	2.0M	94.80	1.04G	5.60M	89.57	37.7M	255K
Last layer RNNPool	95.00	0.334G	2.9M	95.40	3.05G	7.41M	91.14	53.4M	300K
RNNPool Block + Last layer RNNPool	95.60	0.260G	2.7M	95.00	1.26G	6.06M	89.65	37.9M	259K

improves from 2.29 MB to 0.24 MB (if re-computation is disallowed and memory optimization similar to (Chowdhery et al., 2019) is used) and the number of computations slightly improves from 300 MFLOPs to 226 MFLOPs, while the accuracy on ImageNet-10 is retained — 94.4% for the new model vs 94.2% for the base model. These results extend to other networks like EfficientNet, ResNet and GoogLeNet (Szegedy et al., 2015), where residual connection based functional blocks in the initial parts can be effectively replaced with the RNNPoolLayer with improvements in working memory and compute, while retaining comparable accuracy. Table 3 lists these results which are discussed in greater detail in Section 5.

Table 2. MobileNetV2-RNNPool: RNNPoolLayer($R_{in} = 112, C_{in} = 112, S = 4, r = 6, c = 6, k = 32, h_1 = 16, h_2 = 16$) is used. The rest of the layers are defined as in MobileNetV2 (Sandler et al., 2018). Each line denotes a sequence of layers, repeated n times. The first layer of each bottleneck sequence has stride s and rest use stride 1. Expansion factor t is multiplied to the input channels to change the width.

Input	Operator	t	c	n	s
$224^2 \times 3$	conv2d 3 × 3	1	32	1	2
$112^2 \times 32$	RNNPool Block	1	64	1	4
$28^2 \times 64$	bottleneck	6	64	4	2
$14^2 \times 64$	bottleneck	6	96	3	1
$14^2 \times 96$	bottleneck	6	160	3	2
$7^2 \times 160$	bottleneck	6	320	1	2
$7^2 \times 320$	conv2d 1 × 1	1	1280	1	1
$7^2 \times 1280$	avgpool 7 × 7	1	-	1	1
$1 \times 1 \times 1280$	conv2d 1 × 1	1	k	-	1

4.2. Replacement for Pooling Layers

RNNPoolLayer can replace any pooling layer and, in all experiments in this paper, increases the overall accuracy of the network. For example, DenseNet121-RNNPool in Figure 4 has three pooling layers one each in T2, T3, and the final average pool layer. DenseNet121-RNNPool loses

0.6% accuracy compared to the base DenseNet121 model (Table 3). But, replacing all three remaining pooling layers in DenseNet121-RNNPool with a RNNPoolLayer results in almost same accuracy as the base DenseNet121 model while compute and RAM requirement is still about 2× and 4× lower than DenseNet121 model. We can further drop 14 dense layers in D3 and 10 layers in D4 to bring down FLOPs and RAM requirement to 0.79 GFLOPs and 0.43 MB, respectively, while still ensuring 94.2% accuracy.

4.3. New Architectures for Face Detection

Using RNNPoolLayer, we design new architectures for face detection that achieve higher MAP scores than state-of-the-art and are compact enough for real-time face detection on weak microcontrollers. We start with the structure of S3FD (Zhang et al., 2017b), which relates anchor box sizes to the stride of the detection layer. The first detection layer detects the smallest faces and as we go deeper the size of the faces each detection layer predicts increases. Now, instead of applying one convolution layer and then applying RNNPoolLayer, we directly down-sample the image by a factor of 1/4 via RNNPoolLayer. This is critical as for the smallest faces, the anchor box size is set as 16×16 and the required stride is 4. Instead of applying RNNPoolLayer directly on the image, if we use strided convolution first, the MAP for the hard dataset drops significantly. Further, for efficiency, we use depthwise separable convolutions followed by pointwise convolutions before using inverted residual (MBConv) blocks. See Appendix D.2 for a description of our various face detection architectures.

We also create an architecture which can fit within the resource constraints to be deployed on a Cortex M4 microcontroller i.e. it has the peak RAM usage as ≤ 256 KB and inference cost ≤ 128 MFLOPs (latency ≤ 1 s) while having a competitive MAP (Table 5). This is done by creating a model where an RNNPoolLayer of small hidden dimension, $h_1 = h_2 = 4$, is placed after one strided convolution layer and subsequently followed by MBConv blocks. The

first detection head was given a stride of 2 and placed after the first convolution layer, so as to reach a total stride of 4.

5. Evaluation of RNNPool: Vision Tasks

In this section, we present empirical evidence to demonstrate that RNNPool operator is compatible with popular CNN architectures for vision tasks, and can push the envelope of compute and memory usage vs accuracy curve. Further, we show that RNNPool combined with a MobileNet style architecture generates accurate models for Visual Wake Words and face detection problems that can meet the compute and budget requirements of ARM Cortex M4 devices.

Hyperparameters: Models are trained in PyTorch (Paszke et al., 2019) using SGD with momentum optimizer (Sutskever et al., 2013) with weight decay 4×10^{-5} and momentum 0.9. We do data-parallel training with 4 NVIDIA P40 GPUs and use a batch size of 256 for classification and 32 for face detection. We use a cosine learning rate schedule with an initial learning rate of 0.05 for classification tasks, and 0.01 with 5 warmup epochs for face detection tasks. All convolution layers use learnable batch normalization. We use the EdgeML (Dennis et al.) implementation of FastGRNN. More details about hyperparameters can be found in the Appendix D.3

For **inference**, the input image is loaded patch-wise, with the patch size being the receptive field of the output of an RNNPool operator. The outputs of the first convolution layer computed on this patch which overlap with the next patch are stored in memory to avoid re-computation. The output patch of the first convolution is then passed to the RNNPool instance and its output is stored. Thus, the RAM usage corresponds to the volume of the stored computations along with the output of the RNNPool Block. This strategy helps us bring down peak RAM usage to even lower than that of the size of the input image, allowing deployment on devices which cannot even load the whole image in memory.

For calculating **RAM usage** of convolution blocks we follow the strategy of (Chowdhery et al., 2019), which computes it as the output activation map for simple convolutions/pooling operators or the sum of the input and output activation maps for blocks containing residual connections. Using above strategy, the RAM usage of a dense block in DenseNet will just be the output size as it concatenates the input to the output. For Inception blocks (Szegedy et al., 2015), let us consider input to the inception block as I and outputs of each of the 4 paths in the block to be O_1, O_2, O_3 and O_4 . Since we can get rid of the input I after computing the last output, we can order the computation in increasing order of the number of channels in O_i . In this way, the peak RAM while computing the full block will be the sum of input added to the sum of the 3 smallest outputs.

While the above strategy is easiest to implement, there can be better optimization approaches (Pleiss et al., 2017). For example, in DenseNet121 (Figure 4), we can bypass the largest activation map of $56 \times 56 \times 256$ which is the output of D1, by going from output of P1 (O_1) to output of T1 (O_2), by computing it in a sequential manner and storing required intermediate variables only. In particular, we calculate the receptive field of O_2 on O_1 and use the patch with size of this receptive field from O_1 to compute a $1 \times 1 \times 128$ voxel of O_2 . When we do this, we will also have to store intermediate computations that lie in D1 and T1 so that we can avoid re-compute. So the total memory usage here will become $O_1 + O_2$ stored computations, which comes out to be 2.2 MB and is lower than the number reported in Table 3. However, the same strategy can be used for bypassing the output of D3 in DenseNet121-RNNPool and peak RAM can be brought down to 0.56 MB. However, we do not report RAM usage using such complex RAM management techniques as: a) gains are not significant, b) same techniques can be applied to RNNPool, c) they require significant specialization to each architecture.

5.1. RNNPool for Image Classification

We demonstrate that RNNPool can effectively replace large stacks of layers in image classification architectures such as MobileNetV2, EfficientNet-B0, ResNet18, DenseNet121 and GoogLeNet. Here we focus on a 10 class dataset (ImageNet-10) consisting of images from ImageNet-1K (Deng et al., 2009) whose classes correspond to the CIFAR-10 dataset (Krizhevsky et al., 2009). The dataset is divided into 1300 images for training and 50 for validation per class, as in the standard ImageNet-1K. More details about the dataset can be found in the Appendix A.

We first compare RNNPoolLayer against other standard pooling operators and the base network (see Table 1). RNNPool Block corresponds to inserting RNNPoolLayer after the first convolution layer with stride 4 as illustrated in Figure 4 and Table 2. Last layer RNNPool is replacing the global average pooling operation at the end with patch size equal to the input activation’s size (usually 7×7). Finally, RNNPool Block + Last Layer RNNPool corresponds to combining the above two RNNPool replacements.

For different base models, we use different patch and hidden sizes (see Appendix D). All models are trained for 300 epochs and the best top-1 validation accuracy is reported. Table 1 shows that there is a significant accuracy boost using RNNPool as compared to strided convolution, max and average pooling. Replacing the last average pooling layer with RNNPoolLayer further increases accuracy with a minimal increase in model size and FLOPs, thus arguing that RNNPool is a more efficient pooling operator.

Next, Table 3 reports the accuracy of RNNPool when

Table 3. The effect of replacing functional blocks in the baseline models with RNNPoolLayer for ImageNet-10 image classification.

Model	Base						RNNPool			
	Accuracy (%)	Parameters	Memory Optimised		Compute Optimised		Accuracy (%)	Parameters	Peak RAM	FLOPs
			Peak RAM	FLOPs	Peak RAM	FLOPs				
MobileNetV2	94.20	2.20M	0.38 MB	1.00G	2.29 MB	0.30G	94.40	2.00M	0.24 MB	0.23G
EfficientNet-B0	96.00	4.03M	0.40 MB	1.09G	2.29 MB	0.39G	96.40	3.90M	0.25 MB	0.33G
ResNet18	94.80	11.20M	0.76 MB	21.58G	3.06 MB	1.80G	94.40	10.60M	0.49 MB	0.95G
DenseNet121	95.40	6.96M	1.53 MB	24.41G	3.06 MB	2.83G	94.80	5.60M	0.77 MB	1.04G
GoogLeNet	96.00	9.96M	1.63 MB	3.32G	3.06 MB	1.57G	95.60	9.35M	0.78 MB	0.81G

used with various other CNN blocks. The table also compares RNNPool based architectures with the memory and compute-optimized versions of the baseline architectures. For this experiment, the RNNPoolLayer only replaces the blocks after the first convolution; See Table 2 for details of this replacement in MobileNetV2. Compute-optimized refers to the standard inference approach where inference progresses layer-by-layer without any re-computation. The peak RAM usage—computed according to the scheme mentioned above Section 5.1 – of this scheme for the base model is much higher (around 6-8×) than that of the RNNPool models. For memory-optimized inference, we set the peak RAM usage of the baseline model to be slightly higher than that of the RNNPool model, based on which we identify the bottleneck layer. We compute every voxel of this layer by re-computing the required set of convolutions. Similar to compute optimized, we can use a more specialized strategy per architecture to further optimize FLOPs but they do not provide significant savings in general and do not change the main message of the experiment. So, we ignore them in the interest of generality and simplicity of exposition.

Table 3 shows that the FLOPs for DenseNet and ResNet increase significantly as deeper blocks ensure large receptive field thus more inter-voxel dependencies. Overall, we see that RNNPool based models consistently reduce inference cost and model size with comparable accuracies.

Finally, Table 4 presents results on the ILSVRC2012 Imagenet-1K (Deng et al., 2009) dataset with MobileNetV1, MobileNetV2 and EfficientNet-B0 as the baseline models. The new models correspond to Table 2 for MobileNetV2 architecture, and similar replacements for MobileNetV1 and EfficientNet-B0. $h_1 = h_2 = 16$ for the RNNPoolLayer.

Table 4. Comparison of resources and accuracy for ImageNet-1K.

Method	Peak RAM	#Params	FLOPs	Accuracy (%)
MobileNetV1	3.06MB	4.2M	569M	69.52
MobileNetV1-RNNPool	0.77MB	4.1M	417M	69.39
MobileNetV2	2.29MB	3.4M	300M	71.81
MobileNetV2-RNNPool	0.24MB	3.2M	226M	70.14
EfficientNet-B0	2.29 MB	5.3M	390M	76.30
EfficientNet-B0-RNNPool	0.25 MB	5.2M	330M	72.47

We again see a significant decrease in peak RAM usage along with a reduction in FLOPs, while retaining comparable accuracy, except for EfficientNet architecture. EfficientNet uses neural architecture search to optimize the architecture specifically for a given dataset (ImageNet-1K in this case). But for our experiments, we directly replaced certain blocks in EfficientNet without re-optimizing the remaining architecture for ImageNet-1K. We speculate this to be the key reason for accuracy drop and leave further investigation of RNNPool with neural architecture search as a topic for future research.

5.2. RNNPool for Visual Wake Words

The Visual Wake Words challenge (Chowdhery et al., 2019) presents a relevant use case for computer vision on tiny microcontrollers. It requires detecting the presence of a human in the frame with very little resources — no more than 250 KB peak memory usage and model size, and no more than 60 MFLOPs/image. The existing state-of-the-art method (Chowdhery et al., 2019) is MobileNetV2 with a width multiplier of 0.35, 8 channels for the first convolution and 320 channels for the last convolution layer. We use this as our baseline and replace convolutions with an RNNPoolLayer. After training a floating point model with the best validation accuracy, we perform per-channel quantization to obtain 8-bit integer weights and activations.

Table 1 compares the accuracy of the baseline and new architectures on this task. We can increase the accuracy of the base model by more than 1% when replacing the last average pool layer with a RNNPool Block. Inserting RNNPool both at the beginning of the network and at the end, we obtain a solution which is within 0.6% accuracy of the baseline but can provide a significant drop in RAM usage (250 KB → 33.68 KB), model size and FLOPs. We calculate our peak RAM usage using the same memory management technique as (Chowdhery et al., 2019).

Further, we vary input image resolution in {96, 128, 160, 192, 224} to trade-off between accuracy and efficiency. Our memory-accuracy and FLOPs-accuracy curves are significantly higher than the baseline’s curve (Figure 5). For example, the peak RAM usage of MobileNetV2-0.35× with

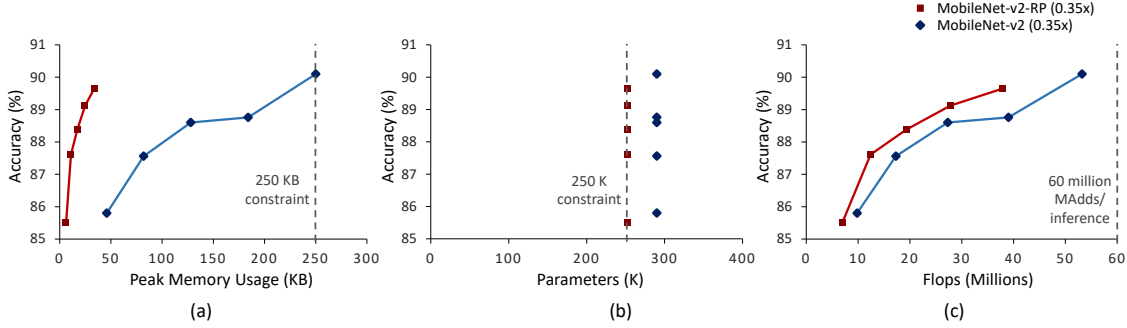


Figure 5. Visual Wake Word: MobileNetV2-RNNPool requires 8× less RAM and 40% less compute than baselines. We cap our number of parameters to be $\leq 250\text{K}$ instead of 290K allowed by MobileNetV2 (0.35×).

Table 5. Comparison of memory requirement, # parameters and validation MAP obtained by different methods for Face Detection on the WIDER FACE dataset. RNNPool-Face-C is able to achieve higher accuracy than the baselines despite using 3× less RAM and 4.5× less FLOPs. RNNPool-Face-Quant enables deployment on Cortex M4 class devices with 6-7% accuracy gains over the cheapest baselines.

Method	Peak RAM	Parameters	FLOPs	MAP			MAP for ≤ 3 faces		
				Easy	Medium	Hard	Easy	Medium	Hard
EagleEye	1.17 MB	0.23M	0.08G	0.74	0.70	0.44	0.79	0.78	0.75
	1.17 MB	0.06M	0.10G	0.77	0.75	0.53	0.81	0.79	0.77
FaceBoxes	1.76 MB	1.01M	2.84G	0.84	0.77	0.39	-	-	-
	1.76 MB	1.12M	1.18G	0.87	0.84	0.67	0.91	0.90	0.88
EXTD	18.75 MB	0.07M	8.49G	0.90	0.88	0.82	0.93	0.93	0.91
	18.75 MB	2.15M	9.25G	0.91	0.88	0.77	0.83	0.83	0.82
	6.44 MB	1.52M	1.80G	0.92	0.89	0.70	0.95	0.94	0.92
RNNPool-Face-Quant	225 KB	0.07M	0.12G	0.80	0.78	0.53	0.84	0.83	0.81

the lowest resolution image is about 40 KB, while our model requires only 34 KB RAM despite using the highest resolution image and ensuring $\approx 4\%$ higher accuracy.

5.3. RNNPool for Face Detection

We create models for real-time face detection with low peak RAM usage. We use the WIDER FACE dataset (Yang et al., 2016) for training and validation. We follow the base structure of S3FD (Zhang et al., 2017b) for creating the detection framework but insert the RNNPool layer at the beginning of the architecture which brings down the image size to 160×120 . RNNPool-Face models use RNNPool blocks of hidden dimensions as 4, 6 and 16 for A, B and C respectively. For, RNNPool-Face-Quant we use a hidden size of 4 with MBConv blocks and quantize the model as in Section 5.2. See Appendix D.2 for a more detailed description of our RNNPool-Face architectures.

Table 5 compares validation Mean Average Precision (MAP) for easy, medium and hard subsets; MAP is a standard metric for face detection and measures the mean area under the precision-recall curve. We also compare computations, number of parameters and peak memory usage of the baseline

real-time face detection models with our RNNPool-Face models (assuming input image size as 640×480). We report MAP scores for baselines based on source code or pre-trained models published by the respective authors. For, Eagle-Eye (Zhao et al., 2019) we wrote our own code to replicate the method in the paper as the source code was not made available. For EXTD, we report FLOPs of the EXTD-32 version, which is computationally cheapest. EXTD and LFFD (He et al., 2019) are accurate but are computationally expensive. In contrast, RNNPool-Face-C achieves better MAP in the easy and medium subsets despite using $\sim 4.5\times$ less compute and $\sim 3\times$ less RAM.

We also compare MAP scores only for images that have ≤ 3 faces, which is a more suitable real-world face-detection setting, especially for tiny devices. Here also, RNNPool-Face-C is more accurate than all the baselines across all the three categories. FaceBoxes (Zhang et al., 2017a) and Eagle-Eye decrease FLOPs and peak memory usage by rapidly down-sampling the image or by decreasing the number of channels significantly, but lead to inaccurate models. In contrast, RNNPool-Face-B and RNNPool-Face-A achieve significantly higher MAPs than these methods while still ensuring smaller FLOPs and peak RAM usage values. A

similar trend holds true when restricted to images with ≤ 3 faces. Finally, RNNPool-Face-Quant uses quantization to ensure a model that can be deployed on Cortex M4 devices which typically have ≤ 256 KB RAM, while still ensuring $> 80\%$ MAP accuracy on images with ≤ 3 faces. Qualitative face detection comparison of the proposed method against the real-time baselines can be found in Figures 6, 7.

6. Conclusions

We proposed RNNPool, an efficient RNN-based non-linear pooling operator. RNNPool operator was used to create RNNPoolLayer which is an effective alternative to the RAM intensive components in modern architectures. The use of RNNPoolLayer reduces peak RAM usage, model size and FLOPs while maintaining or improving accuracy for a variety of vision tasks. Extensive experimentation on Face Detection and Visual Wake Word problems shows that RNNPool based architectures can enable real-time solutions on resource-constrained tiny microcontrollers. Going forward, real-world deployment of RNNPool based solutions for wakeword and similar problems would be of great interest. Also, RNNPool can potentially be combined with more efficient computation graphs over the same architectures. We leave further investigation into optimizing these specific computation graphs as a topic for future research.

Acknowledgements

We are grateful to Sahil Bhatia, Ali Farhadi, Sachin Goyal, Max Horton and Ajay Manchepalli for helpful discussions and feedback. AK did a part of this work during his research fellowship at Microsoft Research India.

References

- Acuna, D., Ling, H., Kar, A., and Fidler, S. Efficient interactive annotation of segmentation datasets with polygon-rnn++. In *Proceedings of the IEEE conference on Computer Vision and Pattern Recognition*, pp. 859–868, 2018.
- Bell, S., Lawrence Zitnick, C., Bala, K., and Girshick, R. Inside-outside net: Detecting objects in context with skip pooling and recurrent neural networks. In *The IEEE Conference on Computer Vision and Pattern Recognition (CVPR)*, June 2016.
- Cai, H., Zhu, L., and Han, S. ProxylessNAS: Direct neural architecture search on target task and hardware. *arXiv preprint arXiv:1812.00332*, 2018.
- Cho, K., Van Merriënboer, B., Gulcehre, C., Bahdanau, D., Bougares, F., Schwenk, H., and Bengio, Y. Learning phrase representations using rnn encoder-decoder for statistical machine translation. *arXiv preprint arXiv:1406.1078*, 2014.

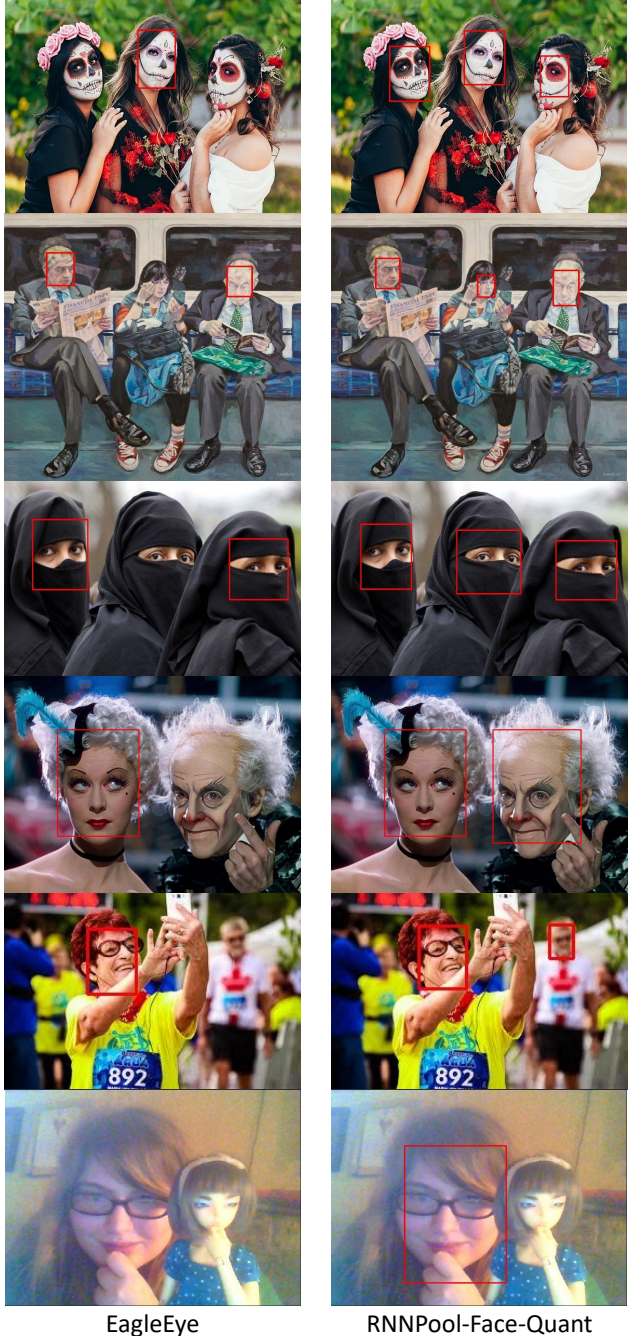


Figure 6. Comparison of performance on test images with EagleEye and RNNPool-Face-Quant. The confidence threshold is set at 0.6 for both models. EagleEye misses faces when there is makeup, occlusion, blurriness and in grainy pictures, while our method is detecting them. However, in the case of some hard faces, RNNPool-Face-Quant still misses a few of them or doesn't give out a bounding box containing the full face.

for statistical machine translation. *arXiv preprint arXiv:1406.1078*, 2014.

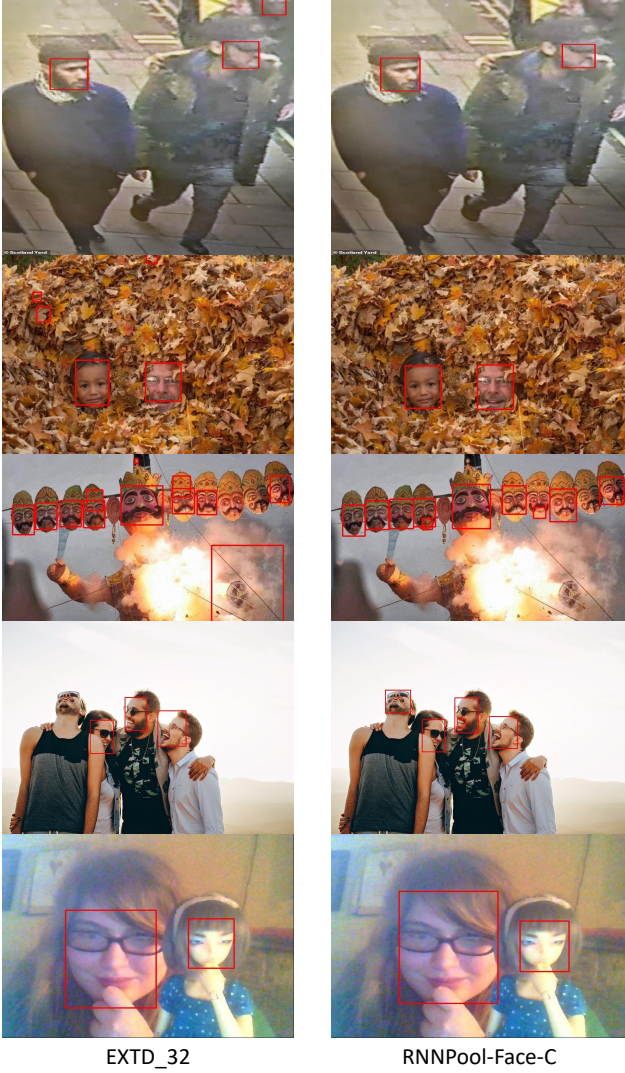


Figure 7. Comparison of performance on test images with EXTD_32 and RNNPool-Face-C. The confidence threshold is set at 0.6 for both models. The EXTD model has more false positives and is also missing more faces. In the first image, EXTD does a faulty prediction at top right. In the image below it EXTD mistakes regions in leaves as faces, while our model detects the two faces only. In the next image, both the models have some wrong detections. But, the EXTD model detects a large bounding box that is a false positive. In the next image EXTD misses a face with unnatural pose which our model detects. However, our model detects a face within a face which in general can be removed easily. In the next image (last row above), both the models detect the two faces, which weren't detected by the models on the left. Our model detects a slightly better bounding box than EXTD.

Cho, M. and Brand, D. Mec: memory-efficient convolution for deep neural network. In *Proceedings of the 34th International Conference on Machine Learning-Volume 70*, pp. 815–824. JMLR. org, 2017.

Chowdhery, A., Warden, P., Shlens, J., Howard, A., and Rhodes, R. Visual wake words dataset. *arXiv preprint arXiv:1906.05721*, 2019.

Deng, J., Dong, W., Socher, R., Li, L.-J., Li, K., and Fei-Fei, L. Imagenet: A large-scale hierarchical image database. In *2009 IEEE conference on computer vision and pattern recognition*, pp. 248–255. Ieee, 2009.

Dennis, D. K., Gaurkar, Y., Gopinath, S., Gupta, C., Jain, M., Kumar, A., Kusupati, A., Lovett, C., Patil, S. G., and Simhadri, H. V. EdgeML: Machine Learning for resource-constrained edge devices. URL <https://github.com/Microsoft/EdgeML>.

Gale, T., Elsen, E., and Hooker, S. The state of sparsity in deep neural networks. *arXiv preprint arXiv:1902.09574*, 2019.

Gong, Y., Wang, L., Guo, R., and Lazebnik, S. Multi-scale orderless pooling of deep convolutional activation features. In *European conference on computer vision*, pp. 392–407. Springer, 2014.

Gural, A. and Murmann, B. Memory-optimal direct convolutions for maximizing classification accuracy in embedded applications. In *International Conference on Machine Learning*, pp. 2515–2524, 2019.

He, K., Zhang, X., Ren, S., and Sun, J. Spatial pyramid pooling in deep convolutional networks for visual recognition. *IEEE transactions on pattern analysis and machine intelligence*, 37(9):1904–1916, 2015.

He, K., Zhang, X., Ren, S., and Sun, J. Deep residual learning for image recognition. In *Proceedings of the IEEE conference on computer vision and pattern recognition*, pp. 770–778, 2016.

He, Y., Xu, D., Wu, L., Jian, M., Xiang, S., and Pan, C. LFFD: A light and fast face detector for edge devices. *arXiv preprint arXiv:1904.10633*, 2019.

Hochreiter, S. and Schmidhuber, J. Long short-term memory. *Neural computation*, 9(8):1735–1780, 1997.

Howard, A. G., Zhu, M., Chen, B., Kalenichenko, D., Wang, W., Weyand, T., Andreetto, M., and Adam, H. Mobilenets: Efficient convolutional neural networks for mobile vision applications. *arXiv preprint arXiv:1704.04861*, 2017.

Huang, G., Liu, Z., Van Der Maaten, L., and Weinberger, K. Q. Densely connected convolutional networks. In *Proceedings of the IEEE conference on computer vision and pattern recognition*, pp. 4700–4708, 2017.

Iandola, F. N., Han, S., Moskewicz, M. W., Ashraf, K., Dally, W. J., and Keutzer, K. SqueezeNet: Alexnet-level

- accuracy with 50x fewer parameters and; 0.5 mb model size. *arXiv preprint arXiv:1602.07360*, 2016.
- Krizhevsky, A., Hinton, G., et al. Learning multiple layers of features from tiny images. 2009.
- Kusupati, A., Singh, M., Bhatia, K., Kumar, A., Jain, P., and Varma, M. FastGRNN: A fast, accurate, stable and tiny kilobyte sized gated recurrent neural network. In *Advances in Neural Information Processing Systems*, pp. 9017–9028, 2018.
- Lai, L., Suda, N., and Chandra, V. Cmsis-nn: Efficient neural network kernels for arm cortex-m cpus. *arXiv preprint arXiv:1801.06601*, 2018.
- LeCun, Y., Bengio, Y., and Hinton, G. Deep learning. *nature*, 521(7553):436–444, 2015.
- Liu, N., Han, J., and Yang, M.-H. Picanet: Learning pixel-wise contextual attention for saliency detection. In *The IEEE Conference on Computer Vision and Pattern Recognition (CVPR)*, June 2018.
- Paszke, A., Gross, S., Massa, F., Lerer, A., Bradbury, J., Chanan, G., Killeen, T., Lin, Z., Gimelshein, N., Antiga, L., et al. Pytorch: An imperative style, high-performance deep learning library. In *Advances in Neural Information Processing Systems*, pp. 8024–8035, 2019.
- Pleiss, G., Chen, D., Huang, G., Li, T., van der Maaten, L., and Weinberger, K. Q. Memory-efficient implementation of densenets. *arXiv preprint arXiv:1707.06990*, 2017.
- Sandler, M., Howard, A., Zhu, M., Zhmoginov, A., and Chen, L.-C. Mobilenetv2: Inverted residuals and linear bottlenecks. In *Proceedings of the IEEE Conference on Computer Vision and Pattern Recognition*, pp. 4510–4520, 2018.
- Sutskever, I., Martens, J., Dahl, G., and Hinton, G. On the importance of initialization and momentum in deep learning. In *International conference on machine learning*, pp. 1139–1147, 2013.
- Szegedy, C., Liu, W., Jia, Y., Sermanet, P., Reed, S., Anguelov, D., Erhan, D., Vanhoucke, V., and Rabinovich, A. Going deeper with convolutions. In *Proceedings of the IEEE conference on computer vision and pattern recognition*, pp. 1–9, 2015.
- Tan, M. and Le, Q. EfficientNet: Rethinking model scaling for convolutional neural networks. In *International Conference on Machine Learning*, pp. 6105–6114, 2019.
- Tan, M., Chen, B., Pang, R., Vasudevan, V., Sandler, M., Howard, A., and Le, Q. V. Mnasnet: Platform-aware neural architecture search for mobile. In *Proceedings of the IEEE Conference on Computer Vision and Pattern Recognition*, pp. 2820–2828, 2019.
- Visin, F., Kastner, K., Cho, K., Matteucci, M., Courville, A., and Bengio, Y. Renet: A recurrent neural network based alternative to convolutional networks. *arXiv preprint arXiv:1505.00393*, 2015.
- Wang, J., Yang, Y., Mao, J., Huang, Z., Huang, C., and Xu, W. CNN-RNN: A unified framework for multi-label image classification. In *Proceedings of the IEEE conference on computer vision and pattern recognition*, pp. 2285–2294, 2016.
- Wang, K., Liu, Z., Lin, Y., Lin, J., and Han, S. Haq: Hardware-aware automated quantization with mixed precision. In *Proceedings of the IEEE conference on computer vision and pattern recognition*, pp. 8612–8620, 2019.
- Xie, W., Noble, A., and Zisserman, A. Layer recurrent neural networks. 2016.
- Xingjian, S., Chen, Z., Wang, H., Yeung, D.-Y., Wong, W.-K., and Woo, W.-c. Convolutional LSTM network: A machine learning approach for precipitation nowcasting. In *Advances in neural information processing systems*, pp. 802–810, 2015.
- Yang, S., Luo, P., Loy, C.-C., and Tang, X. Wider face: A face detection benchmark. In *Proceedings of the IEEE conference on computer vision and pattern recognition*, pp. 5525–5533, 2016.
- Yoo, Y., Han, D., and Yun, S. EXTD: Extremely tiny face detector via iterative filter reuse. *arXiv preprint arXiv:1906.06579*, 2019.
- Zhang, S., Zhu, X., Lei, Z., Shi, H., Wang, X., and Li, S. Z. Faceboxes: A CPU real-time face detector with high accuracy. In *2017 IEEE International Joint Conference on Biometrics (IJCB)*, pp. 1–9. IEEE, 2017a.
- Zhang, S., Zhu, X., Lei, Z., Shi, H., Wang, X., and Li, S. Z. S3fd: Single shot scale-invariant face detector. In *Proceedings of the IEEE International Conference on Computer Vision*, pp. 192–201, 2017b.
- Zhao, Q., Lyu, S., Zhang, B., and Feng, W. Multiactivation pooling method in convolutional neural networks for image recognition. *Wireless Communications and Mobile Computing*, 2018, 2018.
- Zhao, X., Liang, X., Zhao, C., Tang, M., and Wang, J. Real-time multi-scale face detector on embedded devices. *Sensors*, 19(9):2158, 2019.

A. Dataset Information

A.1. ImageNet-10

We created ImageNet-10 by taking images from ILSVRC 2012 ImageNet-1K dataset of 1000 classes. All images corresponding to the 10 classes from CIFAR-10 are sampled from the full dataset. The classes in CIFAR-10 are: airplane, automobile, bird, cat, deer, dog, frog, horse, ship and truck. The corresponding classes chosen from ImageNet-1K are:

1. n02690373: 'airliner'
2. n04285008: 'sports car'
3. n01560419: 'bulbul'
4. n02124075: 'Egyptian cat'
5. n02430045: 'deer'
6. n02099601: 'golden retriever'
7. n01641577: 'bullfrog'
8. n03538406: 'horse cart'
9. n03673027: 'ocean liner'
10. n04467665: 'trailer truck'

The class n02430045: 'deer' is not present in the ImageNet-1K subset and we scraped it from the full ImageNet-22K database. Same number of images are used as in the other classes. Each class is divided into 1300 images for training and 50 images for validation.

A.2. Visual Wake Words

This is a binary classification dataset with the two classes being presence and absence of a person. The dataset is derived by re-labeling the images available in the MS COCO dataset with labels corresponding to whether a person is present or not. The training set has 115K images and the validation set has 8K images. The labels are balanced between the two classes: 47% of the images in the training dataset of 115k images are labeled as person.

A.3. WIDER FACE

This is a face detection dataset having 32,203 images with 393,703 labelled faces varying through scale, pose and occlusion. It is organized based on 61 event classes. Each event class has 40%/10%/50% data as training, validation and testing sets. The images in the dataset are divided into Easy, Medium and Hard cases. The Hard case includes all the images of the dataset, and the Easy and Medium cases both are subsets of Hard case.

B. Experiment Details of testing RNNPool Modelling Power

B.1. Synthetic Experiment Details

We conduct experiments on synthetic datasets to prove that RNNPoolLayer can learn spatial representations. We cre-

ate the following datasets for our experiments (also see Figure 3):

1. A multi-class dataset consisting of images with one line segment of varying lengths and positions. There are 9 classes corresponding to lines ranging from 0 to 160 degrees at 20 degree intervals.
2. A multi-label dataset with images consisting of multiple line segments with varying lengths and positions. There are 9 labels corresponding to lines with orientations of 0 to 160 degrees at 20 degree intervals.
3. A multi-label dataset consisting of images with a subset of shapes – circle, triangle, square, pentagon, hexagon.

We sweep over the h_1, h_2 parameters in powers of 2 and report below the smallest RNNPool operator that can enable a single FC layer to classify or label the test set with 100% accuracy. We do so with and without a preceding CNN layer of 8 convolutions of 3×3 size and stride 2. The table below lists the least h_1, h_2 required for each of the tasks.

Data	Image Size	With Conv.	Without Conv.
(1)	32×32	$h_1 = 4, h_2 = 16$	$h_1 = 16, h_2 = 32$
(2)	32×32	$h_1 = h_2 = 8$	$h_1 = h_2 = 32$
(2)	64×64	$h_1 = 8, h_2 = 16$	$h_1 = h_2 = 32$
(3)	64×64	$h_1 = 8 = h_2 = 16$	$h_1 = h_2 = 32$

B.2. CIFAR-10 Experiment Details

In Section 3.3, we use $h_1 = h_2 = 32$ for the RNNPool operator with patch size and stride as 32. For the strided convolution we use a convolution layer of $4 \times h_2 = 128$ filters. For Max and Average pooling first we pool down to $1 \times 1 \times 3$ from input of $32 \times 32 \times 3$ and then use a 1×1 convolution of 128 filters. All the above have the same patch size and stride size and are followed by a fully connected layer projection to 10 from 128.

C. Details about Compute and Peak RAM Calculation

C.1. RAM Calculations for various block types

1. **MBCConv block** : Give input I of size $H \times W \times C$, a pointwise convolution (C1) first expands the number of channels to $C \times t$ where t is expansion factor. Then there is a depthwise separable 3×3 convolution (C2) with stride either 1 or 2, followed by another pointwise convolution (C3) which reduces the channel to the number of output channels (O) associated with the MBCConv block. To avoid storing the large output (O_{C1}) of C1 and bloating the memory, O_{C1} is

constructed channel by channel, so at first 1 filter of the $C \times t$ filters of C1 will be convolved with I , then this single 2D vector will be convolved by C2. Since C2 is depthwise separable and input channels independently contribute to a output channel, we again get a 2D map. This map is convolved with all filters of C3 and we get an output of O number of channels. We keep doing this, going one by one through each filter of C1 and adding to the output of the MBConv block of O channels, to get the final output. Hence the RAM usage is input added to the output of the MBConv block.

2. **Residual Block** : There is a residual connection, therefore the input activation map has to be store until the output is calculated and then added together. The RAM usage will be sum of input and output in the case of a residual block without stride. Since there is no expansion layer, and no activation map needs to be avoided the RAM usage of a residual block with stride will be $2 \times$ output size, as the input can be downsampled and stored before adding being added to the output.
3. **Dense block** : At any point in a dense block the activation maps to be stored is the input to the dense block and outputs of all previous dense layers, since the last layer needs all the activation maps concatenated as its input. The total activation maps being stored will reach the peak just after the last dense layer. Therefore the peak RAM usage is the output of the dense block.
4. **Inception block** : The peak RAM usage for this has been explained in detail in Section 5. Since no inception layer is strided, we do not need separate case like in residual block.

C.2. Table 3 peak RAM calculations

The peak RAM calculations were done following the strategy of (Chowdhery et al., 2019). The peak RAM of both MobileNetV2 and EfficientNet-B0 are contributed by the first MBConv block in the architecture, while that of the RNNPool versions is the MBConv block right after the RNNPool replacement. According to (Chowdhery et al., 2019), the expanded map in a MBConv block need not be completely stored in the memory if we compute this map channel-by-channel and store the output of the MBConv block contributed by a single channel directly. This can be done as the convolutions inside the MBConv are depthwise separable followed by pointwise. For ResNet18, DenseNet121 and GoogLeNet the bottleneck peak RAM is the activation map just after the first convolution layer. For ResNet18-RNNPool the peak RAM usage is the residual block just after RNNPool i.e. the first residual block out of 2 of conv4_x. For DenseNet121-RNNPool, the peak RAM is the output of D3 (see Figure 4). For GoogLeNet, the

peak RAM is the last inception block on spatial resolution of 14×14 — inception (4e).

C.3. Table 5 peak RAM calculations

For all EagleEye, FaceBoxes, EXTD and LFFD the peak RAM is contributed by the output of the first convolution. For RNNPool-Face-A and RNNPool-Face-B, the peak RAM is the output of the RNNPool, while for RNNPool-Face-C and RNNPool-Face-Quant, it is contributed by the MBConv block right after the RNNPool.

C.4. Table 3 Memory Optimised calculations

As explained above, the RAM calculations for RNNPool based models revealed that the convolution blocks after RNNPoolLayer contribute to the peak RAM (ConvBlock-A). In the memory optimised scheme, we fix the peak RAM of the base model to be that of the convolution block whose RAM usage is bit more than that of RNNPool. This convolution block (ConvBlock-B) naturally comes before ConvBlock-A. ConvBlock-B is chosen such that there exists no block that lies between this block and ConvBlock-A which has a RAM usage less than that of ConvBlock-A. Since we fix the peak RAM, we have to reconstruct an activation map (Activation-A) that comes before ConvBlock-B patch by patch. We do this by loading a patch of the image (one at a time) which is of the size of the receptive field of Activation-A wrt the input image and feed it forward to get a $1 \times 1 \times \text{channel}_{\text{Activation}-A}$ voxel of Activation-A. When we load the next patch we have to re-compute some convolution and pooling outputs which come in the overlapping region of the two again. We keep doing this until we reconstruct Activation-A completely. Note that Activation-A need not necessarily be the activation map just before ConvBlock-B. Activation-A is chosen as the earliest occurring activation map (nearer to input image) which ensures that there is no intermediate layer or block between it and ConvBlock-B which can contribute to more RAM usage. The total FLOPs is calculated as the sum of the FLOPs of the base network and the extra re-computations in order to compute patch-by-patch.

D. Architectures

D.1. Image Classification

D.1.1. RNNPoolLayer IN THE BEGINNING REPLACING MULTIPLE BLOCKS

This kind of replacement is like in Figure 4 and Table 2. The various hidden sizes and patch sizes of RNNPoolLayer in each architecture is given in the table below:

Model	Hidden Size	Patch Size
MobileNetV2-RNNPool	$h_1 = h_2 = 16$	6
EfficientNet-B0-RNNPool	$h_1 = h_2 = 16$	6
ResNet18-RNNPool	$h_1 = h_2 = 32$	8
DenseNet121-RNNPool	$h_1 = h_2 = 48$	8
GoogLeNet-RNNPool	$h_1 = h_2 = 32$	8
MobileNetV2-RNNPool (0.35 \times)	$h_1 = h_2 = 8$	6

Note that the last row refers to the model used for Visual Wake Words experiments.

D.1.2. RNNPoolLayer REPLACING AVERAGE POOLING AT THE END

This kind of replacement in any model resulted in an accuracy improvement. The hidden size of the RNNPool operator is set as $h_1 = h_2 = l/4$ where l is the number of channels in the last activation map before the average pooling. Such a replacement does not contribute to any significant increase in parameters and even less in FLOPs. In Table 1, Row 6 refers to such a replacement in base model and Row 7 to a replacement in RNNPool model (as in D.1.1). In Figure 5, all results of RNNPool are with replacement as in Row 7 in Table 1.

D.1.3. RNNPoolLayer REPLACING INTERMEDIATE POOLING LAYERS

These experiments have been tried on DenseNet121 as base model (Section-4.2), where we are replacing single max-pooling layers appearing in intermediate positions in the network with RNNPool. Given $r_{in} \times c_{in} \times k_{in}$ size input activation map to the pooling layer, the hidden sizes for RNNPool is taken as $h_1 = h_2 = k_{in}/4$, patch size as 4 and stride as 2. Note that we also further drop dense layers (1×1 convolution followed by 3×3 convolution) in D3 and D4. The number of channels in the output of any dense block is sum of number of input channels and output of each dense layer. Hence, reducing number of dense layers reduces the number of channels of the output activation maps of these dense blocks and hence the input to the pooling layer. However, for the RNNPool the same strategy of $h_1 = h_2 = k_{in}/4$ is followed where k_{in} is lesser now.

D.2. Face Detection

We follow the base structure of S3FD (Zhang et al., 2017b) for creating the detection framework. Each RNNPool-Face model is created by placing RNNPool Block directly on input image or after a strided convolution (RNNPool-Face-Quant) and following it by convolution layers or inverted bottleneck residual (MBConv) Blocks. Detection layers are placed at strides of 4, 8, 16, 32, 64 and 128, for square anchor boxes of sizes 16, 32, 64, 128, 256 and 512 as in S3FD. The number of MBConv Blocks or convolution

layers after RNNPool and before each detection layer is decided wrt the required receptive field size of each of the detection layers as defined by S3FD. The detection heads are placed such that they are just before a strided layer in the architecture. The scale compensation anchor matching strategy and max-out background label for small anchor boxes of S3FD are also used. Images are trained on 640×640 images. A multi-task loss is used where cross-entropy loss is used for classification of anchor box and smooth L1 loss is used as regression loss for bounding box coordinate offsets. We use multi-scale testing and Non-Maximal Suppression during inference to determine final bounding boxes.

Following is the architecture of RNNPool-Face-C. There is a detection layer after every bottleneck stack. The detection layer is two 3×3 heads which predict the class probability (2 outputs per pixel) and bounding box offsets(4 outputs per pixel). The convention followed in the table below is same as in Table 2. t is the expansion coefficient, c is the number of output channels, n is the number of repetitions of the MBConv² layer and s is the stride associated with the first of those stack of layers. RNNPool has $h_1 = h_2 = 16$.

Input	Operator	t	c	n	s
$640 \times 480 \times 3$	RNNPoolLayer	1	64	1	4
$160 \times 120 \times 64$	bottleneck	6	24	2	1
$160 \times 120 \times 24$	bottleneck	6	32	3	2
$80 \times 60 \times 32$	bottleneck	6	64	4	2
$40 \times 30 \times 64$	bottleneck	6	96	3	2
$20 \times 15 \times 96$	bottleneck	6	160	2	2
$10 \times 7 \times 160$	bottleneck	6	320	1	2

Architecture for RNNPool-Face-B is as follows. The detection heads are after the second row of the table and then after each stack of bottleneck layers. RNNPool has $h_1 = h_2 = 6$.

Input	Operator	t	c	n	s
$640 \times 480 \times 3$	RNNPoolLayer	1	24	1	4
$160 \times 120 \times 24$	conv2d 3 \times 3	1	24	4	1
$160 \times 120 \times 24$	conv2d 3 \times 3	1	96	1	2
$80 \times 60 \times 96$	conv2d 1 \times 1	1	32	1	1
$80 \times 60 \times 32$	bottleneck	6	32	3	1
$80 \times 60 \times 32$	bottleneck	6	64	3	2
$40 \times 30 \times 64$	bottleneck	6	128	2	2
$20 \times 15 \times 128$	bottleneck	6	160	1	2
$10 \times 7 \times 160$	bottleneck	6	320	1	2

Architecture for RNNPool-Face-A is as follows. The detection heads are after the second row of the table and then after each stack of bottleneck layers. RNNPool has

²We use the terms 'bottleneck', MBConv and inverted residual interchangeably, they refer to the same block.

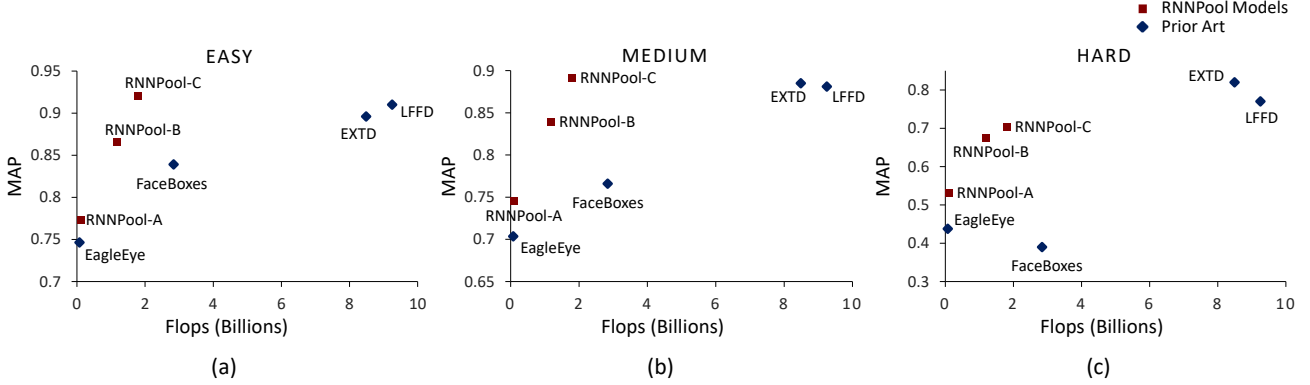


Figure 8. Visualization of FLOPs reduction vs MAP of RNNPool models wrt Prior Art for Face Detection on WIDER Face Dataset

$h_1 = h_2 = 4$. Depthwise+Pointwise refers to a depthwise separable 3×3 convolution followed by a pointwise 1×1 convolution.

Input	Operator	t	c	n	s
$640 \times 480 \times 3$	RNNPoolLayer	1	16	1	4
$160 \times 120 \times 16$	Depthwise+Pointwise	1	16	4	1
$160 \times 120 \times 16$	Depthwise+Pointwise	1	16	1	2
$80 \times 60 \times 16$	bottleneck	1	16	3	1
$80 \times 60 \times 16$	bottleneck	1	24	3	2
$40 \times 30 \times 24$	bottleneck	1	32	2	2
$20 \times 15 \times 32$	bottleneck	2	128	1	2
$10 \times 7 \times 128$	bottleneck	2	160	1	2

Architecture for RNNPool-Face-Quant is as follows. The detection heads are after the second row of the table and then after each stack of bottleneck layers. The first detection head has a strided 3×3 convolution so as to reach a total stride of 4 (following S3FD). RNNPool has $h_1 = h_2 = 4$.

Input	Operator	t	c	n	s
$640 \times 480 \times 3$	conv2d 3×3	1	4	1	2
$320 \times 240 \times 4$	conv2d 3×3	1	4	1	2
$320 \times 240 \times 4$	RNNPoolLayer	1	16	1	4
$80 \times 60 \times 16$	bottleneck	2	16	4	1
$80 \times 60 \times 16$	bottleneck	2	24	4	2
$40 \times 30 \times 24$	bottleneck	2	32	2	2
$20 \times 15 \times 32$	bottleneck	2	64	1	2
$10 \times 7 \times 64$	bottleneck	2	96	1	2

The RNNPool models decrease FLOPs drastically while maintaining performance. Figure 8, shows the difference we are making. In <2 GFLOPs we are getting easy and medium MAP better than EXTD and LFFD which are near to 10 GFLOPs.

D.3. FastGRNN Hyperparameters

We use FastGRNN as both the RNNs in RNNPool. We usually use same hidden dimension for both the RNNs. We fix ζ as 1 and ν as 0 for all models, for stability, and use piecewise linear non-linearities quantTanh and quantSigmoid for the Visual Wake Word models, so we can quantize it without loss of information.

E. Augmentations

Various image augmentations were used for training each network. For the ImageNet experiments the training images were cropped to random size of 0.08 to 1.0 times the original size and reshaped to a random aspect ratio of 3/4 to 4/3. This was then resized to 224×224 . This image was further flipped horizontally randomly and then normalized by mean and standard deviation. For the validation set, we resize the input image to 256×256 and then take a center crop of 224×224 . For the Visual Wake Word experiment, we follow a similar process except during training we crop the input image first to a random size of 0.2 to 1.0 times the original size. For varying resolutions from 96 to 224 as reported in Figure 5, the ratio of resize resolution of input image and center crop size is kept same during validation. All other augmentations are kept same with output size changed from 96 to 224. For Face Detection experiments we use augmentations like in S3FD (Zhang et al., 2017b). This includes colour distortion, random cropping : specifically zooming in to smaller faces to get more larger faces to train on, and horizontal flipping after cropping to 640×640 . Note that the same augmentation strategies were used for the baseline models also for fair comparison.